Highly Active Oxygen Reduction Electrocatalysts Derived from an Iron-Porphyrin Framework

Mark C. Elvington,[1,*,§§§] Prabhu Ganesan,[1,2,†] Patrick A. Ward,[2,‡] Jian Liu,[3,§,§§§] Ahmet Atilgan,[3,¶] Boris V. Kramar,[3,**] Karren More,[4,††] David Cullen,[4,‡‡] Joseph T. Hupp,[3,§§] Scott Greenway,[1,¶¶] W. Taylor Adams IV,[2,***] and Héctor R. Colón-Mercado[2,†††]

[1] *Greenway Energy, 301 Gateway Drive, Aiken, South Carolina 29803, USA*

[2] *Savannah River National Laboratory, Aiken, South Carolina, 29808, USA*

[3] *Department of Chemistry, Northwestern University, Evanston, Illinois, 60208, USA*

[4] *Center for Nanophase Materials Sciences, Oak Ridge National Laboratory, Oak Ridge, Tennessee, 37831-6064, USA*

(Received 3 May 2023; accepted 24 August 2023; published 25 October 2023)

The high cost of noble metals is a barrier to widespread commercialization of polymer electrolyte membrane fuel cells. Platinum-group-metal-free catalysts are a promising low-cost alternative for catalyzing the oxygen reduction reaction (ORR). Herein, we report a high activity Fe-N-C cathode catalyst derived from a Fe-porphyrinic framework prepared using low-cost precursors and facile one pot synthesis followed by a single heat treatment. The final product has atomically dispersed iron in proximity to nitrogen groups that share transition metal characteristics, as described by electron energy loss spectrometry and x-ray absorption near edge structure results. Electrochemical studies on a rotating ring-disk electrode indicate a four-electron transfer mechanism for the ORR. Membrane electrode assembly testing of the Fe-porphyrin-derived cathode catalyst shows a high kinetic current density of 22 mA cm^{-2} at 0.9 V in H_2-O_2 fuel cells.

DOI: 10.1103/PRXEnergy.2.043008

I. INTRODUCTION

Commercial proliferation of polymer electrolyte membrane fuel cell (PEMFC) technology is limited by cathode catalyst performance, due to the sluggish kinetics of the oxygen reduction reaction (ORR) [1,2]. Platinum and Pt-alloy catalysts are typically utilized, as they generally show high ORR activity and stability in PEMFCs [3–5]. However, the high cost and scarcity of platinum has motivated the development of platinum-group-metal-(PGM) free cathode catalysts. Tremendous advances have been made in PGM-free catalyst development over the past decade following Jasinski's pioneering efforts, which showed remarkable ORR activity for cobalt phthalocyanine in 25% KOH [6].

A variety of synthesis approaches have been reported for PGM-free catalysts composed of transition metals (TMs), a carbon source, and a nitrogen source; followed by high temperature pyrolysis under an inert atmosphere [7–15]. Irrespective of the wide variety of catalyst synthesis procedures employed, the end product can be generalized as TM-N-C-type catalysts with TM-N_x coordination complex moieties [11]. In early PGM-free catalyst development, a typical practice was to impregnate iron and/or cobalt- and nitrogen-containing precursors onto high surface area carbon followed by pyrolysis under an inert atmosphere (mostly nitrogen) at elevated temperatures [9,10,16–18]. However, an improvement in the ORR activity was reported for an Fe-N-C catalyst prepared using

*marke@transitionenergyinc.com
†prabhu.ganesan@srnl.doe.gov
‡patrick.ward@srnl.doe.gov
§kjlsch@rit.edu
¶ahmet.atilgan@u.northwestern.edu
**boriskramar2023@u.northwestern.edu
††morekl1@ornl.gov
‡‡cullenda@ornl.gov
§§j-hupp@northwestern.edu
¶¶scott@greenway-energy.com
***william.adams@srnl.doe.gov
†††hector.colon-mercado@srnl.doe.gov
‡‡‡Current location: Transition Energy LLC, 1228 Gordon Hwy, Augusta, Georgia, 30901, USA
§§§Current location: Rochester Institute of Technology, 1 Lomb Memorial Drive, Rochester, New York, 14623, USA

a silica template approach [19,20]. The past decade witnessed the emergence of a series of PGM-free catalysts derived from polyaniline (PANI) [7,21,22], [cyanamide (CM) + PANI]-Fe-N-C [23] metal organic frameworks (MOFs) [24–26], zeolitic imidazolate frameworks (ZIFs) [14,27–29], covalent organic frameworks [30], and porphyrin [31,32] precursors, where the polymer or framework precursors account for all the carbon and nitrogen prior to the pyrolysis step.

Catalysts prepared from the pyrolysis of MOFs showed significant ORR activities; however, some preparation methods showed low product yields [24,25]. The Fe-based catalyst prepared by polymerizing aniline onto an oxidized carbon support, followed by pyrolysis at 900 °C under a nitrogen atmosphere, showed excellent ORR activity and stability [7]. Further improvements were reported for this catalyst by adding cyanamide [12] and zinc chloride [33] during synthesis or by utilizing bimetallic TM-N-C catalysts [20,34–36]. Recent reports on the development of Fe-N-C catalysts describe the presence of atomically dispersed Fe that exhibit higher ORR activity at 0.9 $V_{iR\text{-free}}$ [11,37–39]. Damjanović *et al*. showed the effect of catalyst loading on the mass activity of a commercial Fe-N-C catalyst [40]. Their study indicated that the mass activity was not affected over a wide range of loadings in both H_2/O_2 fuel cells and rotating ring-disk electrode (RRDE) studies. Besides Fe and Co, an entirely new class of PGM-free catalysts based on Mn, having high ORR activity and stability, has also been reported [41–43]. However, many of the highest activity catalysts require a large number of synthesis steps, and in some cases, the yields are low.

Here, we report an alternative route for the facile synthesis of ORR active FeN_4-type catalysts prepared from Fe-poly-phenylporphyrin precursors that rival the performance of other Fe-N-C-type catalysts. With ongoing research devoted to improving PGM-free catalysts for automotive applications, the present work provides a high throughput synthesis route for producing PGM-free catalysts from inexpensive starting materials having high ORR activity.

II. EXPERIMENTAL DETAILS

A. Poly-phenylporphyrin-based catalyst synthesis

The poly-phenylporphyrin synthesis was adapted from the work published by Kong *et al*. [32] and described in the Supplemental Material [44]. Following the framework synthesis, a reddish-brown product was dried in a vacuum oven at 90 °C for 12 h prior to the pyrolysis step. Pyrolysis was performed at temperatures ranging from 850 to 1000 °C using a rapid heating profile heat treatment, whereby the sample was moved from a room temperature zone to the pyrolysis zone in about 1 s. After pyrolysis for a predefined period of time (between 5 and 15 min), the sample was moved from the heated zone into the room temperature zone. Pyrolysis was performed under anhydrous ammonia, with typical catalyst yields ranging from 40 to 50%, depending on the heat treatment conditions. Compared to a traditional heat treatment method, a ramp heat treatment was also performed with a 10 °C min^{-1} ramp rate and a dwell time of 1 h under a flow of high purity argon. After completion, the sample was allowed to cool to room temperature.

B. Physical characterization

The as-prepared and pyrolyzed poly-phenylporphyrin-based materials were characterized using a variety of techniques. The Brunauer-Emmett-Teller (BET) surface area was measured by using N_2 adsorption-desorption measurements at 77 K on a Micromeritics Tristar II 3020 instrument. Each sample was activated at 120 °C for 12 h under high vacuum on a Smart Vacprep instrument from Micromeritics. Approximately 30 mg of sample was used for each surface area measurement. The BET surface area was calculated in the region $P/P_0 = 0.005$–0.05. Thermogravimetric analysis (TGA) and residual gas analysis (RGA) measurements were carried out on a Perkin Elmer TGA8000 instrument contained in a Vac Atmospheres argon filled glovebox. TGA was integrated with a Hiden Halo 201 residual gas analyzer via a heated capillary transfer line, which was held at 120 °C. 2–3 mg of the as-prepared porphyrinic framework was heated at a ramp rate of 50 °C min^{-1} from 30 to 950 °C and held at 950 °C for 15 min under argon and ammonia atmospheres as purge gases over the sample. C, H, and N elemental analyses were performed using an Elementar Vario-El Cube analyzer. Transmission electron microscopy (TEM) and scanning electron microscopy (SEM) imaging were conducted using a Hitachi HF-3300 instrument operated at 300 kV. Scanning transmission electron microscopy (STEM) and STEM-based electron energy loss spectroscopy (EELS) experiments were performed using an aberration-corrected Nion UltraSTEM instrument operated at 60 kV. The electron microscopes are accessible through an approved user proposal at the Center for Nanophase Materials Sciences (CNMS) at Oak Ridge National Laboratory and are key capabilities of the ElectroCat Consortium. X-ray photoelectron spectroscopy (XPS) measurements were conducted at the KECKII/NUANCE facility at Northwestern University using a Thermo Scientific ESCALAB 250 Xi (Al $K\alpha$ radiation, $h\nu = 1486.6$ eV) instrument equipped with an electron flood gun. XPS data were analyzed using Thermo Scientific Avantage Data System software, and all spectra were referenced to the C 1*s* peak (284.8 eV).

1. Inductively coupled plasma atomic emission spectroscopy (ICP-AES)

ICP-AES was conducted on a Varian Vista-MDX model ICP-AES spectrometer (Varian, Walnut Creek, CA)

equipped with a CCD detector and an argon plasma. Samples (∼10 mg) were digested in a small amount (1 ml) of a mixture of 3:1 v/v concentrated H_2SO_4:H_2O_2 (30 wt % in H_2O) by heating in a Biotage (Uppsala, Sweden) SPX microwave reactor (software version 2.3, build 6250) at 150 °C for 5 min. The acidic solution was then diluted to a final volume of 15 ml with ultrapure deionized H_2O.

2. X-ray absorption data analysis

X-ray absorption spectroscopy (XAS) measurements at the Fe *K*-edge were performed on the beamline of the DuPont-Northwestern-Dow Synchrotron Research Center (DND-CAT Sector 5-BM) at the Advanced Photon Source at Argonne National Laboratory. Iron foil was used as the reference; calibration was performed with iron foil and reference iron oxides (FeO, Fe_2O_3). Data collected for the as-prepared and pyrolyzed samples had to be deglitched as demonstrated below; deglitching was performed using the in-built functionality of the Demeter XAS analysis suite, i.e., the faulty regions were cut out of the data and the terminal points on both sides of the glitch were connected by a straight line. We recognize that the deglitching procedure at this scale has a significant impact on the results of any quantitative analysis; in fact, fitting experimental data to theoretical standards could not be carried out with sufficient precision, as reflected by the obtained uncertainties on parameter estimates.

C. Electrochemical characterization and fuel cell testing

All electrochemical measurements were performed on a PINE research bipotentiostat (WaveDriver 20) equipped with a high-speed rotator. A PINE research RRDE (AFMSRCE rotator with E6R2 tip, from Pine Research Instrumentation, USA), with a glassy carbon disk (5.61 mm diameter) and platinum ring (7.92 mm OD and 6.25 mm ID), was used as a working electrode. A graphite rod was used as the counter electrode and a reversible hydrogen electrode (RHE) was used as the reference electrode. Catalyst dispersions, hereafter referred to as inks, were prepared by mixing the catalyst powder (11.1 mg) and 5 wt % Nafion® solution (D520, Alfa Aesar) in an ice-cold sonication bath for 30 min followed by stirring overnight. Catalyst films were prepared by drop-casting the ink onto the glassy carbon disk and dried under air for 10 min at room temperature. The target loading for all catalyst films was 600 $\mu g\,cm^{-2}$. For comparison, platinum on high surface area carbon (45.6% Pt/C, Tanaka Kikinzoku Kogyo K.K, TEC-10E50E) was used with a platinum loading target of 20 $mg\,cm^{-2}$. All cyclic voltammetry (CV) and ORR polarization data were recorded in 0.1 *M* $HClO_4$ electrolyte, prepared from 70% perchloric acid (GFS Chemicals, Veritas double distilled) and deionized (DI) water. Typical electrochemical characterization consisted of an initial break-in CV period (CV, 50 full cycles under O_2) followed by two full CV cycles (50–1100 mV vs RHE) recorded at 900 and 1600 rpm, and finally a chronoamperometry protocol for 2 min at 800 mV versus RHE. The ORR currents measured at 800 mV are reported herein. Due to slow cathode kinetics, potential step voltammetry (PSV) was used to obtain accurate steady-state polarization plots. Using 20 mV 30 s step increments allowed the non-Faradaic capacitive current to dissipate, enabling accurate Faradaic measurements. The two electron ORR product, hydrogen peroxide, was measured by using a Pt ring electrode with an applied potential of 1.1 V versus RHE.

Half membrane electrode assemblies (MEAs) were prepared by applying the anode catalysts onto a Nafion membrane. The anode catalyst ink was prepared using a commercial Pt/C catalyst (45.6% Pt/C, Tanaka Kikinzoku Kogyo K.K, TEC-10E50E), DI water, and isopropanol. Catalyst coated membranes were prepared by depositing the anode ink onto a Nafion membrane (NRE 212) using ultrasonic spray coating (Prism-400BT, Ultrasonic Systems, Inc.). The anode loading was kept at 0.15 mg/cm^2. The cathode catalyst ink was prepared by mixing the polyphenylporphyrin-based catalyst with D520 Nafion dispersion (1:1 wt %) in an ice-cold sonication bath for 30 min. The cathode ink was hand brushed onto the half MEA at 80 °C to achieve a PGM-free catalyst loading of 6 mg/cm^2. The MEA was then assembled into a 5 cm^2 single cell assembly using carbon cloths as gas diffusion layers and silicone rubber gaskets. The single cell was evaluated between open circuit potential and 0.3 V using an Arbin Instruments fuel cell station. Testing was performed at 80 °C using hydrogen and oxygen (200 and 200 sccm) at 100% relative humidity.

III. RESULTS AND DISCUSSION

A. Electrochemical screening of pyrolysis conditions

The heat treatment conditions were selected according to the electrochemical results obtained using an RRDE. As described in Sec. II, the catalyst films were cycled in oxygen, after which the potential was held at 800 mV for 2 min. The current measured at the end of the 2 min potential hold is shown in Fig. 1. The first experimental variable that was evaluated was the effect of gas used during pyrolysis of the poly-phenylporphyrin catalyst precursor material. As observed in Fig. 1, an Ar heat treatment results in poor catalyst performance with progressively lower activity at higher pyrolysis temperatures. A similar study was performed using a flow of pure ammonia that resulted in a significant improvement in performance, with a maximum in activity occurring between 950 and 1000 °C. However, high temperature pyrolysis and a longer reaction time under ammonia significantly reduced the catalyst yield. Because ammonia is highly

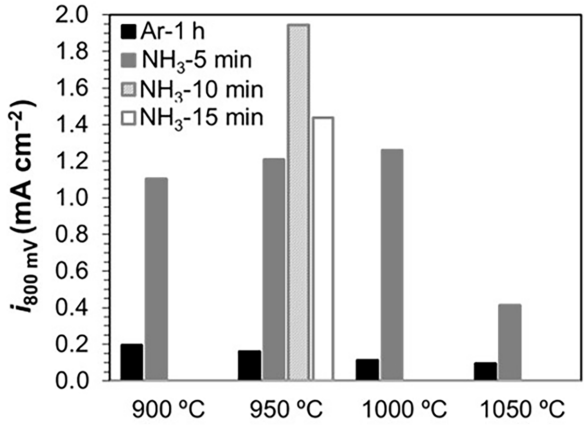

FIG. 1. Electrochemical screening of the ORR activity for various heat treatment conditions. Data collected after being held for 2 min at 800 mV versus RHE at a rotation speed of 900 rpm in O_2 saturated 0.1 *M* $HClO_4$ at a catalyst disk loading of 600 μg cm^{-2}.

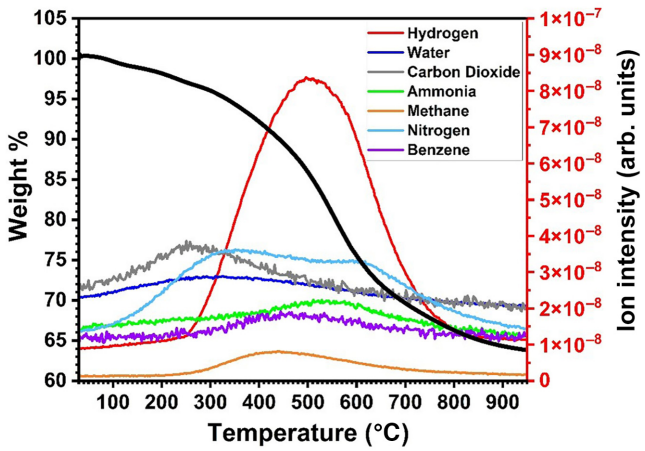

FIG. 2. TGA and RGA of as-prepared poly-phenylporphyrin framework under argon flow at 50 °C min^{-1} from 30 to 950 °C. (Scale of ion intensities for the following ions were increased for clarity: nitrogen ×2, carbon dioxide ×10, ammonia ×5, benzene ×10.)

reactive, several pyrolysis times were studied at 950 °C. Data indicate that 10 min of pyrolysis time is sufficient to activate the poly-phenylporphyrin framework for the ORR. In conclusion, data indicate that activation heat treatment in ammonia for 10 min at 950 °C is optimal for this PGM-free catalyst.

B. Physical characterization

To better understand the activation process and influence that ammonia gas has at high temperatures during the heat treatment of the poly-phenylporphyrin framework, TGA and RGA measurements were conducted under argon and ammonia atmospheres. The as-prepared porphyrinic framework heated under an argon atmosphere produced decomposition products including pyrrole, benzene, nitrogen, hydrogen, ammonia, methane, and carbon dioxide. Figure 2 illustrates substantial hydrogen release during decomposition under an argon atmosphere as well as the release of trace amounts of hydrocarbons and ammonia.

To simulate the synthesis process, the as-prepared material was rapidly heated to 950 °C and held at this temperature for 15 min under argon and ammonia atmospheres. Figure 3 highlights a significant increase in decomposition and weight loss for the sample in the presence of ammonia as compared to argon. Also, hydrogen and nitrogen generated from the autodecomposition of ammonia gas are present in high concentrations at the target activation temperature of 950 °C. It should be noted that alumina crucibles were used and the platinum furnace cover and crucibles were removed to prevent possible catalyzed reactions from platinum.

The as-prepared poly-phenylporphyrin sample, which consisted of the synthesized material prior to heat treatment, and a heat-treated sample (ammonia atmosphere at 950 °C for 10 min) were analyzed by electron microscopy methods. SEM imaging [Fig. 4(a)] shows that the as-prepared and heat-treated particles are approximately the same size, around 150–200 nm in diameter. The as-prepared particles appear dense, have smooth surfaces, and show amorphous internal consistency. TEM images of the as-prepared catalyst particles show no evidence of Fe-containing clusters or particles [Fig. 4(b)]. After heat treatment, the large carbon particles appear rough, are mesographitic, and exhibit nanoporosity [Fig. 4(c)]. STEM imaging, in conjunction with EELS [Figs. 4(d) and 4(e)], shows the presence of atomically dispersed Fe atoms, with the Fe atoms visible at the basal plane edges and steps and in proximity to N. No Fe-containing atom clusters are observed in the STEM images for the heat-treated particles [Fig. 4(e)].

XPS, CHN, and ICP-AES analyses were used to characterize the bulk and surface compositions of the prepared materials, before and after pyrolysis. The results indicate that the bulk concentration of iron in the as-prepared sample is less than 0.1 at. % (see Table S3 within the Supplemental Material [44]). The nitrogen content, in contrast, is very high, at 10–11 at. %, roughly corresponding to the theoretical N concentration of the polymer matrix. After pyrolysis, an increase in the amount of iron to 0.38 at. % is observed due to the decomposition of the porphyrinic framework. This is expected, as no Fe should be lost during the pyrolysis step. On the other hand, the nitrogen content is reduced to around 5 at. %, about half of the as-prepared value. Even with this loss of nitrogen, it can be assumed that most of the nitrogen is undersaturated, from the theoretical amount of iron per nitrogen in the catalyst material.

Figure 5 shows the N 1*s* spectrum for the as-prepared material and the pyrolyzed poly-phenylporphyrin catalyst. Prior to pyrolysis, nearly all of the nitrogen is pyrrolic,

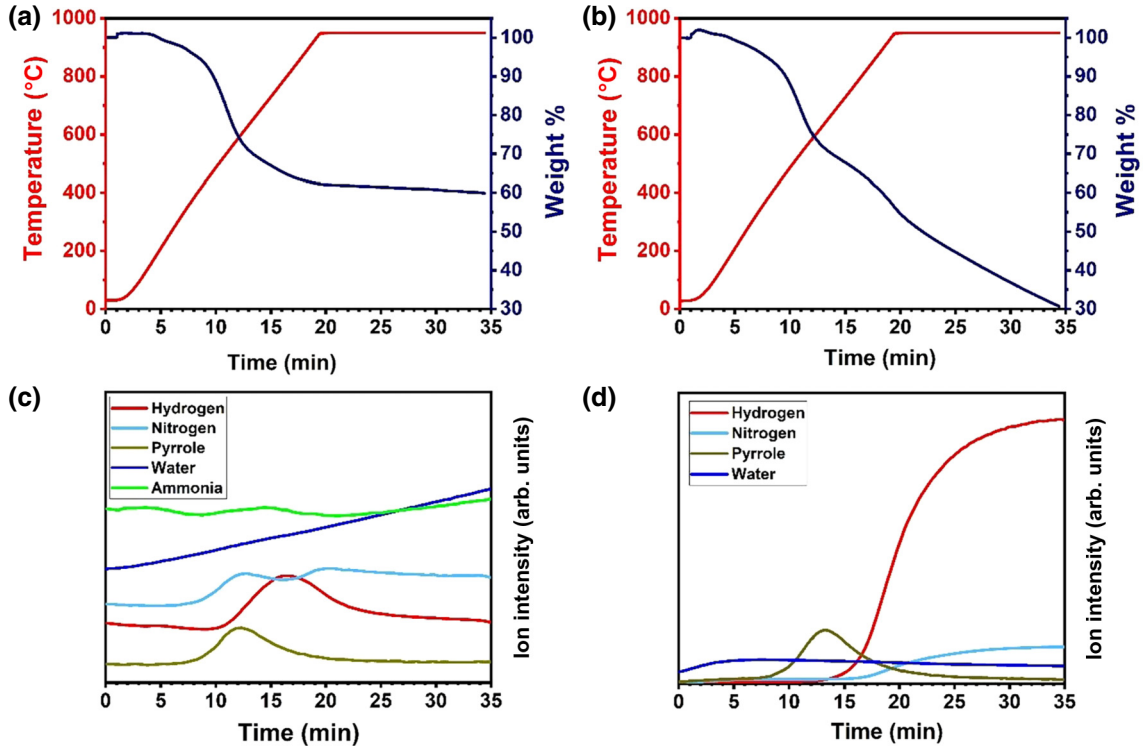

FIG. 3. TGA of as-prepared poly-phenylporphyrin framework (a) under argon flow and (b) under anhydrous ammonia flow. RGA of as-prepared poly-phenylporphyrin framework (c) under argon flow (scale of ion intensities for the following ions were increased for clarity: nitrogen ×5, pyrrole ×10) and (d) under anhydrous ammonia flow (scale of ion intensities for the following ions were altered for clarity: hydrogen divided by 20, nitrogen divided by 20, water divided by 10, pyrrole ×10).

as expected in a porphine-centric material. Following pyrolysis, a significant increase in pyridinic N is observed, with the ratio of pyridinic and pyrrolic N now approximately 1:1, along with a small amount of graphitic and quaternary N.

XAS measurements were conducted to better understand the local and chemical structures of the as-prepared and pyrolyzed samples. Figure 6(a) shows x-ray absorption near edge structure (XANES) data plotted for the samples of interest, structural references [an iron(III)-porphyrin sample and iron foil], and oxidation state references [iron(II) and iron(III) oxides]. The position of the white line with respect to observations for FeO and Fe_2O_3 show that Fe in the as-prepared sample is present strictly in the 3+ oxidation state. The broadened nature of the white line for the pyrolyzed sample suggests that the iron is present as a mixture of 3+, 2+, and 0 oxidation states.

Satisfactory precision of the fitting parameters for the Fe *K*-edge extended x-ray absorption fine structure (EXAFS) could not be obtained due to the necessity to extensively deglitch the samples and the limited useful *k*-range (see Figs. S3 and S4 within the Supplemental Material [44]) [45–47]. However, a qualitative comparison to relevant reference samples was informative with regard to the chemical nature of the as-prepared and pyrolyzed samples [Fig. 6(b)]. The local structure around the Fe absorber in the as-prepared sample is similar to that of an iron-porphyrin sample (for fitting parameters, see Fig. S5 and Table S1 within the Supplemental Material [44]), while the local structure around the Fe absorber in the pyrolyzed sample can be successfully reproduced with both Fe-N and Fe-Fe scattering paths. The presence of higher order scattering paths for the pyrolyzed sample suggests that Fe nanoparticles are forming, rather than nanoclusters (see fitting parameters in Fig. S6 and Table S2 within the Supplemental Material [44]). These conclusions are further supported by the XANES preedge regions [Fig. 6(a)]. The as-prepared sample displays a single preedge peak corresponding to the $1s \rightarrow 3d$ transition; its intensity and full-width at half-maximum are identical to the same preedge peak observed for the Fe-porphyrin reference. At the same time, the preedge for the pyrolyzed sample contains a transition with a metallic character.

C. Electrochemical characterization

Electrochemical analysis of the pyrolyzed poly-phenylporphyrin-based catalyst with an RRDE shows a high oxygen reduction performance. Prior to pyrolysis, the as-prepared sample was a poor conductor and exhibited little or no ORR performance (data not shown). The polarization curve, obtained using a potential step method,

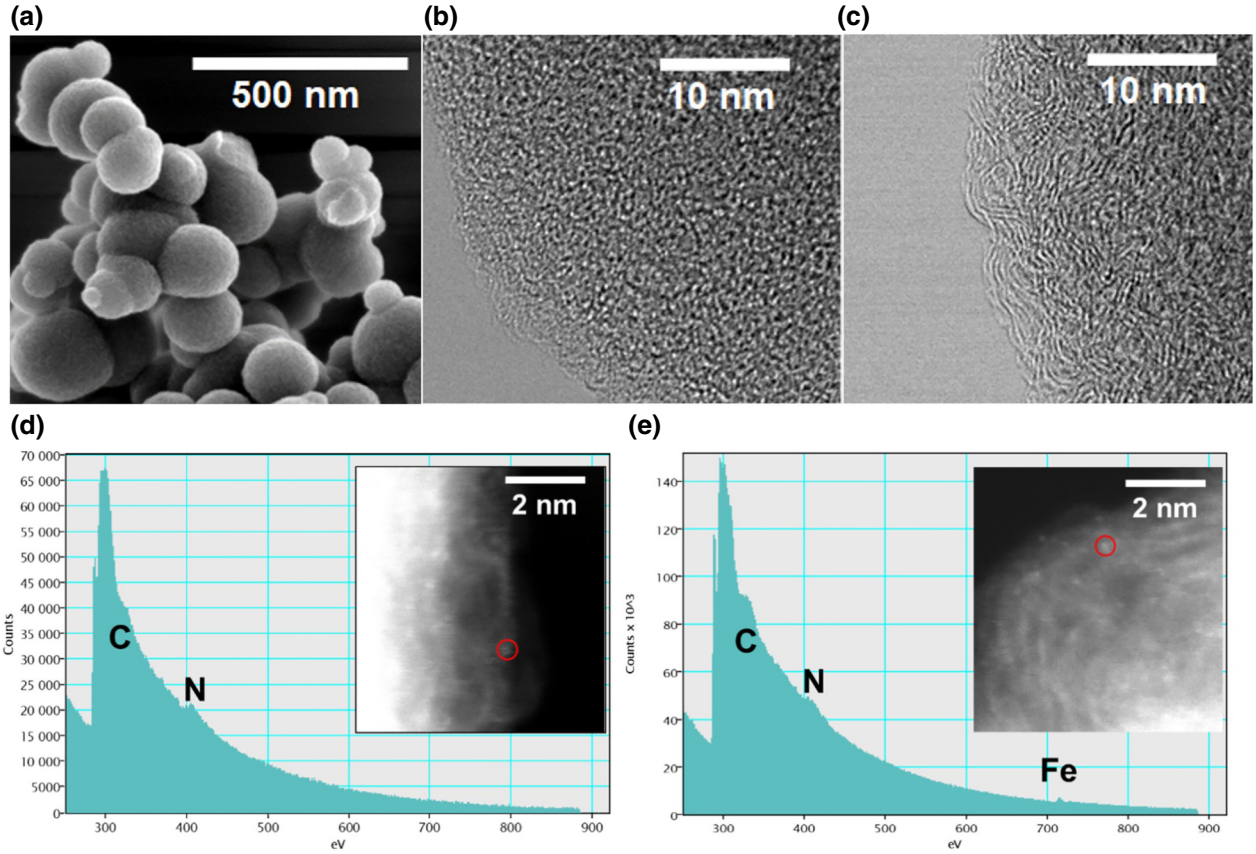

FIG. 4. (a) SEM image of the poly-phenylporphyrin particles after pyrolysis. (b) TEM image of single particle of optimized as-prepared poly-phenylporphyrin. (c) TEM image of single particle after pyrolysis. (d) Point EELS spectra from analysis of as-prepared poly-phenylporphyrin and after pyrolysis (e), with STEM image inset. Analysis spot indicated by red circles in (d),(e).

showed an $E_{1/2}$ of 0.815 V versus RHE [Fig. 7(a)] for the pyrolyzed catalyst. For comparison, the ORR performance of commercial Pt/C, which shows an $E_{1/2}$ of 0.91 V versus RHE, is also included in the figure. Using the optimized synthesis conditions described in Sec. II, the catalyst achieved high current densities at 0.8 V (2.56 mA cm^{-2}) and 0.9 V (0.56 mA cm^{-2}). A recent report showed that a porphyrin-based Fe/N/C catalyst did not exhibit any ORR activity at 0.8 V for a comparable catalyst loading (500 μg cm^{-2}) [48]; however, similar ORR activity at 0.8 V was reported for catalysts derived from Co-porphyrin [49]. Table S4 within the Supplemental Material [44] compares the ORR performance of the porphyrin-derived catalyst developed here with those reported in the literature

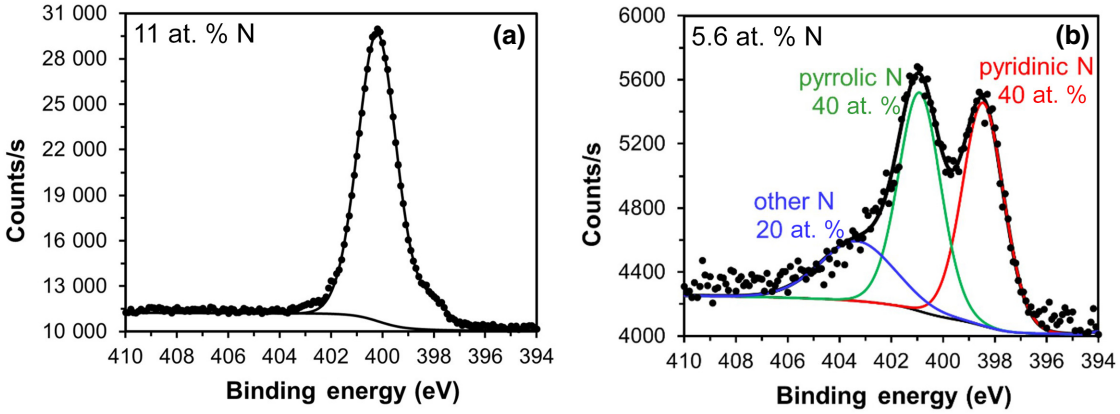

FIG. 5. XPS N 1*s* spectra for poly-phenylporphyrin based catalysts for (a) as-prepared material and (b) after pyrolysis.

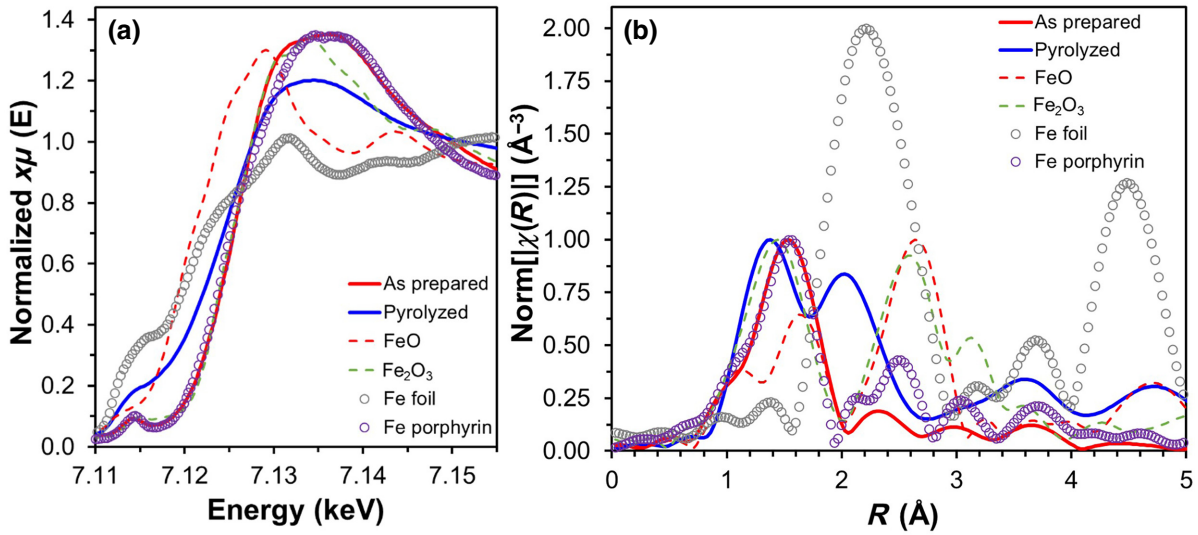

FIG. 6. (a) Fe K-edge XANES results for conventional poly-phenylporphyrin as-prepared and after pyrolysis compared to other Fe moieties in +2 and +3 oxidation states. Relevant reference samples are plotted as scatter plots, bulk oxides as dashed lines, and as-prepared and pyrolyzed samples are shown by solid lines. (b) Fe K-edge EXAFS results for poly-phenylporphyrin showing as-prepared and after pyrolysis samples compared with several reference materials. Data for all samples were normalized to 1, except for Fe foil, which were normalized to 2 to reflect the higher relative intensity of metal-metal scattering. It is readily observed that the as-prepared sample is porphyrinic in nature, while the pyrolyzed sample contains significant metal-metal scattering extending to higher shells.

[5,13,18,50]. Analysis of the ring current indicates high selectivity for the four electron oxygen reduction pathway. An H_2O_2 yield of <3% was obtained for all potentials within the range of 0.05–0.80 V, which equated to >3.93 electrons transferred per O_2.

MEAs were prepared using the pyrolyzed catalyst and tested in a H_2/O_2 fuel cell test station. Conditions optimized for low current density operation were selected to evaluate the initial and short-term catalytic behavior of the catalyst. These conditions include a high ionomer concentration (50 wt %), high catalyst loadings (~6 mg cm^{-2}), and 100% relative humidity. Figure 7(b) shows the initial activity polarization curve with and without iR correction. A high open circuit potential (OCP) of 0.97 V was observed. Below the OCP, a current density of 22 mA cm^{-2} at 900 mV$_{iR\text{-free}}$ (18.5 mA cm^{-2} at 900 mV), and 150 mA cm^{-2} at 800 mV$_{iR\text{-free}}$ (88 mA cm^{-2} at 800 mV), was measured. However, at current densities above 225 mA cm^{-2}, significant mass transport limitations are observed. After the initial performance evaluation, the catalyst was subjected to a 700 mV potential hold. The fuel cell performance reported here for the one-pot synthesized poly-phenylporphyrin catalyst is much higher than those reported in the literature for porphyrin-based catalysts. In fact, most of the studies did not show activity at 0.9 V due to the poor OCP [51,52]. Cantillo *et al.* [51] showed an OCP below 0.9 V for the microporous iron(III)-porphyrin framework derived cathode catalyst that exhibited a relatively low current density ($\leq 2 \times 10^5$ A cm^{-2}) above 0.7 V and 0.1 A cm^{-2} at 0.6 V.

Data showing current density decay as a function of time are shown in Fig. S7(b) within the Supplemental Material [44]. As indicated in the figure, there is an initial increase in performance during the first 2 h of operation. After this initial increase, the current decayed in an exponential fashion until the experiment was terminated after approximately 50 h of operation. The polarization was measured from the OCP to 0.3 V every hour. Figure S7(c) within the Supplemental Material [44] shows a kinetic current decay at 900 mV$_{iR\text{-free}}$. Even though the 700 mV potential hold experiment demonstrated an initial increase in performance, an immediate decay in performance was observed in the high potential region. In contrast to the 700 mV potential hold, the high potential current density decays in a logarithmic fashion. At the end of the experiment, only 25% of the initial performance remains. In contrast, the current density at the end of the 700 mV potential hold is about 46% of the peak current density. Similar performance losses, up to 50% within the initial few hours, were reported for Fe/N/C-type catalysts derived from various precursors, including ZIFs [27,53], polyporphyrins [54,55], and various polymers [56,57]. We recognize that the degradation rate of the porphyrin-derived catalyst is quite high; however, the objective of the present study is the facile synthesis of a highly active PGM-free cathode catalyst for a PEMFC, and the reported approach provides an alternative route and molecular platform to develop PGM-free catalysts. The polymer framework can be easily modified to add functional groups to modify the pyrolysis product. With similar optimization approaches to those

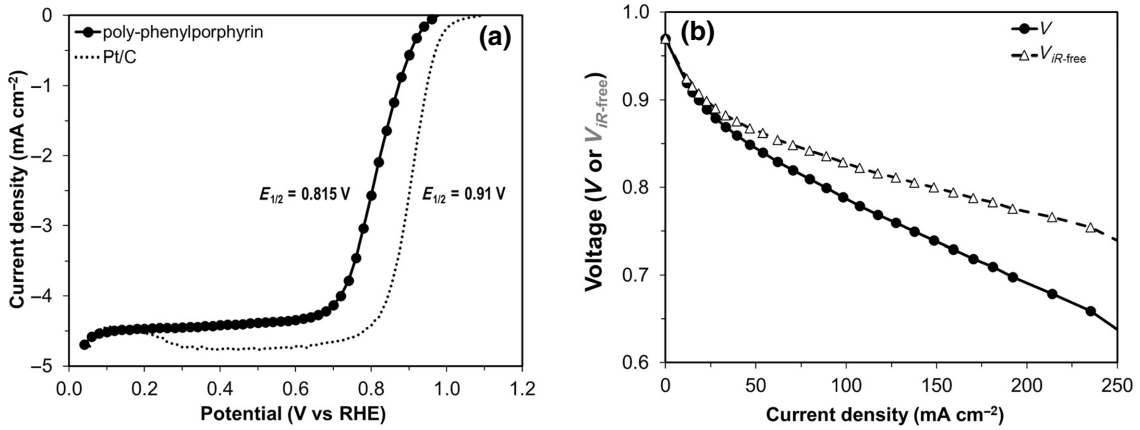

FIG. 7. (a) Oxygen reduction performance for a pyrolyzed poly-phenylporphyrin catalyst. $E_{1/2}$ of 0.815 V versus RHE was measured from the PSV (anodic). Data were collected using PSV at a rotation speed of 900 rpm in a O_2 saturated 0.1 M $HClO_4$ and a catalyst disk loading of 600 $\mu g\,cm^{-2}$ for the poly-phenylporphyrin and 20 $\mu g_{Pt}\,cm^{-2}$ for commercial Pt/C. (b) H_2/O_2 fuel cell performance of catalysts derived from poly-phenylporphyrin.

taken for more commonly studied catalysts, such as MOF-based ones [8], it is possible to improve the stability of the poly-phenylporphyrin based catalyst while maintaining high activity.

IV. CONCLUSION

A poly-phenylporphyrin derived Fe-C-N_x catalyst with a high surface area and excellent ORR activity at 0.9 $V_{iR\text{-free}}$ was synthesized using simple synthesis and pyrolysis steps. TEM and STEM imaging, in conjunction with EELS, of the pyrolyzed catalyst revealed a mesographitic structure with nanoporosity and atomically dispersed Fe atoms at the basal plane edges in close proximity to N. XAS studies indicated the presence of Fe in the +3 oxidation state for the as-prepared and pyrolyzed poly-phenylporphyrin samples. Furthermore, EXAFS analysis showed no Fe-Fe bonding and Fe present as single atom sites in the as-prepared and pyrolyzed poly-phenylporphyrin samples. RRDE studies indicated high selectivity for the ORR, and H_2-O_2 fuel cell studies showed a high OCP and a current density of 22.4 mA cm^{-2} at 0.9 $V_{iR-\text{free}}$ for the optimized catalyst.

The Department of Energy will provide public access to these results of federally sponsored research in accordance with the DOE Public Access Plan [58].

ACKNOWLEDGMENTS

Funding was provided by the US DOE Office of Energy Efficiency and Renewable Energy, Hydrogen and Fuel Cell Technologies Office, under the ElectroCat Consortium, DOE technology managers D. Peterson and D. Papageorgopolous. Microscopy research was performed at Oak Ridge National Laboratory's CNMS, which is a U.S. Department of Energy, Office of Science User Facility. This work made use of the Advanced Photon Source of Argonne National Laboratory (ANL), at DND-CAT (Sector 5), which is supported by E.I. DuPont de Nemours & Co., Northwestern University, and The Dow Chemical Co. This work made use of KECK II facilities of Northwestern University's NUANCE Center, which has received support from the Soft and Hybrid Nanotechnology Experimental (SHyNE) Resource (NSF ECCS-1542205). This work made use of the IMSERC facility at Northwestern University, which has received support from the NSF (CHE-1048773 and DMR-0521267). This work was produced by Battelle Savannah River Alliance, LLC under Contract No. 89303321CEM000080 with the U.S. Department of Energy.

[1] W. S. Jung and B. N. Popov, Hybrid cathode catalyst with synergistic effect between carbon composite catalyst and Pt for ultra-low Pt loading in PEMFCs, Catal. Today **295**, 65 (2017).

[2] Y.-J. Wang, W. Long, L. Wang, R. Yuan, A. Ignaszak, B. Fang, and D. P. Wilkinson, Unlocking the door to highly active ORR catalysts for PEMFC applications: Polyhedron-engineered Pt-based nanocrystals, Energy Environ. Sci. **11**, 258 (2018).

[3] H. A. Gasteiger, S. S. Kocha, B. Sompalli, and F. T. Wagner, Activity benchmarks and requirements for Pt, Pt-alloy, and non-Pt oxygen reduction catalysts for PEMFCs, Appl. Catal., B **56**, 9 (2005).

[4] B. Han, C. E. Carlton, A. Kongkanand, R. S. Kukreja, B. R. Theobald, L. Gan, R. O'Malley, P. Strasser, F. T. Wagner, and Y. Shao-Horn, Record activity and stability of dealloyed bimetallic catalysts for proton exchange membrane fuel cells, Energy Environ. Sci. **8**, 258 (2015).

[5] W. Chen, Q. Xiang, T. Peng, C. Song, W. Shang, T. Deng, and J. Wu, Reconsidering the benchmarking evaluation of catalytic activity in oxygen reduction reaction, iScience **23**, 101532 (2020).

[6] R. Jasinski, A new fuel cell cathode catalyst, Nature **201**, 1212 (1964).

[7] G. Wu, K. L. More, C. M. Johnston, and P. Zelenay, High-performance electrocatalysts for oxygen reduction derived from polyaniline, iron, and cobalt, Science **332**, 443 (2011).

[8] F. Jaouen, E. Proietti, M. Lefèvre, R. Chenitz, J.-P. Dodelet, G. Wu, H. T. Chung, C. M. Johnston, and P. Zelenay, Recent advances in non-precious metal catalysis for oxygen-reduction reaction in polymer electrolyte fuel cells, Energy Environ. Sci. **4**, 114 (2011).

[9] V. Nallathambi, J. W. Lee, S. P. Kumaraguru, G. Wu, and B. N. Popov, Development of high performance carbon composite catalyst for oxygen reduction reaction in PEM proton exchange membrane fuel cells, J. Power Sources **183**, 34 (2008).

[10] N. P. Subramanian, X. G. Li, V. Nallathambi, S. P. Kumaraguru, H. Colon-Mercado, G. Wu, J. W. Lee, and B. N. Popov, Nitrogen-modified carbon-based catalysts for oxygen reduction reaction in polymer electrolyte membrane fuel cells, J. Power Sources **188**, 38 (2009).

[11] H. T. Chung, D. A. Cullen, D. Higgins, B. T. Sneed, E. F. Holby, K. L. More, and P. Zelenay, Direct atomic-level insight into the active sites of a high-performance PGM-free ORR catalyst, Science **357**, 479 (2017).

[12] H. T. Chung, C. M. Johnston, K. Artyushkova, M. Ferrandon, D. J. Myers, and P. Zelenay, Cyanamide-derived non-precious metal catalyst for oxygen reduction, Electrochem. Commun. **12**, 1792 (2010).

[13] W. Shi, Y.-C. Wang, C. Chen, X.-D. Yang, Z.-Y. Zhou, and S.-G. Sun, A mesoporous Fe/N/C ORR catalyst for polymer electrolyte membrane fuel cells, Chin. J. Catal. **37**, 1103 (2016).

[14] W. Sun, L. Du, Q. Tan, J. Zhou, Y. Hu, C. Du, Y. Gao, and G. Yin, Engineering of nitrogen coordinated single cobalt atom moieties for oxygen electroreduction, ACS Appl. Mater. Interfaces **11**, 41258 (2019).

[15] R. M. Torres, M. Sun, R. Yuan, M. Abdelrahman, Z. Guo, T. Kowalewski, K. Matyjaszewski, P. R. LeDuc, and S. Litster, Fe-doped copolymer-templated nitrogen-rich carbon as a PGM-free fuel cell catalyst, ACS Appl. Energy Mater. **4**, 9653 (2021).

[16] G. Liu, X. G. Li, P. Ganesan, and B. N. Popov, Development of non-precious metal oxygen-reduction catalysts for PEM fuel cells based on N-doped ordered porous carbon, Appl. Catal., B **93**, 156 (2009).

[17] R. Bashyam and P. Zelenay, A class of non-precious metal composite catalysts for fuel cells, Nature **443**, 63 (2006).

[18] G. Wu, C. M. Johnston, N. H. Mack, K. Artyushkova, M. Ferrandon, M. Nelson, J. S. Lezama-Pacheco, S. D. Conradson, K. L. More, D. J. Myers, *et al.*, Synthesis-structure-performance correlation for polyaniline-Me-C non-precious metal cathode catalysts for oxygen reduction in fuel cells, J. Mater. Chem. **21**, 11392 (2011).

[19] A. Serov, K. Artyushkova, and P. Atanassov, Fe-N-C oxygen reduction fuel cell catalyst derived from carbendazim: Synthesis, structure, and reactivity, Adv. Energy Mater. **4**, 1301735 (2014).

[20] T. Reshetenko, M. Odgaard, G. Randolf, K. K. Ohtaki, J. P. Bradley, B. Zulevi, X. Lyu, D. A. Cullen, C. J. Jafta, A. Serov, *et al.*, Design of PGM-free cathodic catalyst layers for advanced PEM fuel cells, Appl. Catal., B **312**, 121424 (2022).

[21] Z. Qiao, H. G. Zhang, S. Karakalos, S. Hwang, J. Xue, M. J. Chen, D. Su, and G. Wu, 3D polymer hydrogel for high-performance atomic iron-rich catalysts for oxygen reduction in acidic media, Appl. Catal., B **219**, 629 (2017).

[22] L. Bai, J. Liu, C. Jin, J. Zhang, and F. Wang, Heteroatom-doped carbon interpenetrating networks: A signpost to achieve the best performance of non-PGM catalysts for fuel cells, J. Mater. Chem. A **8**, 18767 (2020).

[23] S. T. Thompson, A. R. Wilson, P. Zelenay, D. J. Myers, K. L. More, K. C. Neyerlin, and D. Papageorgopoulos, ElectroCat: DOE's approach to PGM-free catalyst and electrode R&D, Solid State Ionics **319**, 68 (2018).

[24] K. Strickland, E. Miner, Q. Jia, U. Tylus, N. Ramaswamy, W. Liang, M.-T. Sougrati, F. Jaouen, and S. Mukerjee, Highly active oxygen reduction non-platinum group metal electrocatalyst without direct metal-nitrogen coordination, Nat. Commun. **6**, 7343 (2015).

[25] X. J. Wang, H. G. Zhang, H. H. Lin, S. Gupta, C. Wang, Z. X. Tao, H. Fu, T. Wang, J. Zheng, G. Wu, *et al.*, Directly converting Fe-doped metal organic frameworks into highly active and stable Fe-N-C catalysts for oxygen reduction in acid, Nano Energy **25**, 110 (2016).

[26] L. Du, L. Xing, G. Zhang, and S. Sun, Metal-organic framework derived carbon materials for electrocatalytic oxygen reactions: Recent progress and future perspectives, Carbon **156**, 77 (2020).

[27] D. Zhao, J. L. Shui, L. R. Grabstanowicz, C. Chen, S. M. Commet, T. Xu, J. Lu, and D. J. Liu, Highly efficient non-precious metal electrocatalysts prepared from one-pot synthesized zeolitic imidazolate frameworks, Adv. Mater. **26**, 1093 (2014).

[28] S. Q. Ma, G. A. Goenaga, A. V. Call, and D. J. Liu, Cobalt imidazolate framework as precursor for oxygen reduction reaction electrocatalysts, Chem. - Eur. J. **17**, 2063 (2011).

[29] H. Chen, S. You, Y. Ma, C. Zhang, B. Jing, Z. Cai, B. Tang, N. Ren, and J. Zou, Carbon thin-layer-protected active sites for ZIF-8-derived nitrogen-enriched carbon frameworks/expanded graphite as metal-free catalysts for oxygen reduction in acidic media, Chem. Mater. **30**, 6014 (2018).

[30] C.-Y. Lin, D. Zhang, Z. Zhao, and Z. Xia, Covalent organic framework electrocatalysts for clean energy conversion, Adv. Mater. **30**, 1703646 (2018).

[31] S. Bruller, H. W. Liang, U. I. Kramm, J. W. Krumpfer, X. L. Feng, and K. Mullen, Bimetallic porous porphyrin polymer-derived non-precious metal electrocatalysts for oxygen reduction reactions, J. Mater. Chem. A **3**, 23799 (2015).

[32] A. Kong, Y. Zhang, Z. Chen, A. Chen, C. Li, H. Wang, and Y. Shan, One-pot synthesized covalent porphyrin polymer-derived core-shell Fe_3C@carbon for efficient oxygen electroreduction, Carbon **116**, 606 (2017).

[33] P. Zelenay and D. Myers, in *Proceedings of the Hydrogen and Fuel Cells Program: 2017 Annual Merit Review and Peer Evaluation Meeting*, Washington, DC, (2017).

[34] M. Gollasch, J. Müller-Hülstede, H. Schmies, D. Schonvogel, P. Wagner, A. Dyck, and M. Wark, Elucidating synergistic effects of different metal ratios in

bimetallic Fe/Co-N-C catalysts for oxygen reduction reaction, Catalysts **11**, 841 (2021).

[35] M. Kodali, C. Santoro, S. Herrera, A. Serov, and P. Atanassov, Bimetallic platinum group metal-free catalysts for high power generating microbial fuel cells, J. Power Sources **366**, 18 (2017).

[36] F. Luo, S. Wagner, I. Onishi, S. Selve, S. Li, W. Ju, H. Wang, J. Steinberg, A. Thomas, U. I. Kramm, *et al.*, Surface site density and utilization of platinum group metal (PGM)-free Fe–NC and FeNi–NC electrocatalysts for the oxygen reduction reaction, Chem. Sci. **12**, 384 (2021).

[37] H. G. Zhang, S. Ding, S. Hwang, X. L. Zhao, D. Su, H. Xu, H. P. Yang, and G. Wu, Atomically dispersed iron cathode catalysts derived from binary ligand-based zeolitic imidazolate frameworks with enhanced stability for PEM fuel cells, J. Electrochem. Soc. **166**, F3116 (2019).

[38] Y. Cheng, J. Zhang, X. Wu, C. Tang, S. Z. Yang, P. P. Su, L. Thomsen, F. Zhao, S. F. Lu and J. Liu, A template-free method to synthesis high density iron single atoms anchored on carbon nanotubes for high temperature polymer electrolyte membrane fuel cells, Nano Energy **80**, 105534 (2021).

[39] Y. H. He, S. W. Liu, C. Priest, Q. R. Shi, and G. Wu, Atomically dispersed metal-nitrogen-carbon catalysts for fuel cells: Advances in catalyst design, electrode performance, and durability improvement, Chem. Soc. Rev. **49**, 3484 (2020).

[40] A. M. Damjanović, B. Koyutürk, Y. S. Li, D. Menga, C. Eickes, H. A. El-Sayed, H. A. Gasteiger, T. P. Fellinger, and M. Piana, Loading impact of a PGM-free catalyst on the mass activity in proton exchange membrane fuel cells, J. Electrochem. Soc. **168**, 114518 (2021).

[41] H. Xu, in *Proceedings of the Hydrogen and Fuel Cells Program: 2019 Annual Merit Review and Peer Evaluation Meeting*, April, 29 2019, Arlington, VA, (2019).

[42] K. Liu, Z. Qiao, S. Hwang, Z. Liu, H. Zhang, D. Su, H. Xu, G. Wu, and G. Wang, Mn- and N-doped carbon as promising catalysts for oxygen reduction reaction: Theoretical prediction and experimental validation, Appl. Catal., B **243**, 195 (2019).

[43] M. Chen, X. Li, F. Yang, B. Li, T. Stracensky, S. Karakalos, S. Mukerjee, Q. Jia, D. Su, G. Wang, *et al.*, Atomically dispersed MnN_4 catalysts via environmentally benign aqueous synthesis for oxygen reduction: Mechanistic understanding of activity and stability improvements, ACS Catal. **10**, 10523 (2020).

[44] See the Supplemental Material at http://link.aps.org/supplemental/10.1103/PRXEnergy.2.043008 for synthesis information and additional data.

[45] M. Hideki, T. Tooru, O. Kenji, S. Hiroshi, and M. Masayasu, The crystal and molecular structure of diaqua(tetraphenylporphinato)cobalt(III) perchlorate, Bull. Chem. Soc. Jpn. **55**, 4 (1982).

[46] F.S. Klaus Muller-Buschbaum, CCDC 1037410: Experimental Crystal Structure Determination. (2014).

[47] A. Ertl, S. Ralf, Stefan Prowatke, Franz Brandstätter, Thomas Ludwig, Heinz-Jürgen Bernhardt, Friedrich Koller, and John M. Hughes, Mn-rich tourmaline and fluorapatite in a Variscan pegmatite from Eibenstein an der Thaya, Bohemian massif, Lower Austria, Eur. J. Mineral. **16**, 551 (2004).

[48] L. Ni, P. Theis, S. Paul, R. W. Stark, and U. I. Kramm, *In situ* 57Fe Mössbauer study of a porphyrin based FeNC catalyst for ORR, Electrochim. Acta **395**, 139200 (2021).

[49] C. Li, Z. Han, Y. Yu, Y. Zhang, B. Dong, A. Kong, and Y. Shan, Efficient oxygen electroreduction over ordered mesoporous Co-N-doped carbon derived from cobalt porphyrin, RSC Adv. **6**, 15167 (2016).

[50] M. Z. Sun, S. Y. Gong, Y. X. Zhang, and Z. Q. Niu, A perspective on the PGM-free metal-nitrogen-carbon catalysts for PEMFC, J. Energy Chem. **67**, 250 (2022).

[51] N. M. Cantillo, G. A. Goenaga, W. Gao, K. Williams, C. A. Neal, S. Ma, K. L. More, and T. A. Zawodzinski, Investigation of a microporous iron(III) porphyrin framework derived cathode catalyst in PEM fuel cells, J. Mater. Chem. A **4**, 15621 (2016).

[52] S. Samireddi, V. Aishwarya, I. Shown, S. Muthusamy, S. M. Unni, K. T. Wong, K. H. Chen, and L. C. Chen, Synergistic dual-atom molecular catalyst derived from low-temperature pyrolyzed heterobimetallic macrocycle-N4 corrole complex for oxygen reduction, Small **17**, 2103823 (2021).

[53] E. Proietti, F. Jaouen, M. Lefevre, N. Larouche, J. Tian, J. Herranz, and J. P. Dodelet, Iron-based cathode catalyst with enhanced power density in polymer electrolyte membrane fuel cells, Nat. Commun. **2**, 416 (2011).

[54] W. Wang, Q. Y. Jia, S. Mukerjee, and S. L. Chen, Recent insights into the oxygen-reduction electrocatalysis of Fe/N/C Materials, ACS Catal. **9**, 10126 (2019).

[55] S. W. Yuan, J. L. Shui, L. Grabstanowicz, C. Chen, S. Commet, B. Reprogle, T. Xu, L. P. Yu, and D. J. Liu, A highly active and support-free oxygen reduction catalyst prepared from ultrahigh-surface-area porous polyporphyrin, Angew. Chem., Int. Ed. **52**, 8349 (2013).

[56] Y. C. Wang, Y. J. Lai, L. Song, Z. Y. Zhou, J. G. Liu, Q. Wang, X. D. Yang, C. Chen, W. Shi, Y. P. Zheng, *et al.*, S-Doping of an Fe/N/C ORR catalyst for polymer electrolyte membrane fuel cells with high power density, Angew. Chem., Int. Ed. **54**, 9907 (2015).

[57] J. Y. Choi, L. J. Yang, T. Kishimoto, X. G. Fu, S. Y. Ye, Z. W. Chen, and D. Banham, Is the rapid initial performance loss of Fe/N/C non precious metal catalysts due to micropore flooding?, Energy Environ. Sci. **10**, 296 (2017).

[58] http://energy.gov/downloads/doe-public-access-plan.